Title

Short-interval estimation of proliferation rate using serial diffusion MRI predicts progression-free survival in newly diagnosed glioblastoma treated with radiochemotherapy

Journal

Journal of Neuro-Oncology, 116(3)

ISSN

0167-594X

Authors

Zaw, Taryar M
Pope, Whitney B
Cloughesy, Timothy F
et al.

Publication Date

2014-02-01

DOI

10.1007/s11060-013-1344-7

Peer reviewed

Published in final edited form as:
J Neurooncol. 2014 February ; 116(3): 601–608. doi:10.1007/s11060-013-1344-7.

Short-interval estimation of proliferation rate using serial diffusion MRI predicts progression-free survival in newly diagnosed glioblastoma treated with radiochemotherapy

Taryar M. Zaw, B.S.[1], **Whitney B. Pope, M.D., Ph.D.**[1], **Timothy F. Cloughesy, M.D.**[2], **Albert Lai, M.D., Ph.D.**[2], **Phioanh L. Nghiemphu, M.D.**[2], and **Benjamin M. Ellingson, Ph.D.**[1,3,4]

[1] Department of Radiological Sciences, David Geffen School of Medicine, University of California Los Angeles, Los Angeles, CA

[2] Department of Neurology, David Geffen School of Medicine, University of California Los Angeles, Los Angeles, CA

[3] Biomedical Physics, David Geffen School of Medicine, University of California Los Angeles, Los Angeles, CA

[4] Department of Bioengineering, Henry Samueli School of Engineering and Applied Science, University of California Los Angeles, Los Angeles, CA

Abstract

Cell invasion, motility, and proliferation level estimate (CIMPLE) mapping is a new imaging technique that provides parametric maps of microscopic invasion and proliferation rate estimates using serial diffusion MRI data. However, a few practical constraints have limited the use of CIMPLE maps as a tool for estimating these dynamic parameters, particularly during short-interval follow-up times. The purpose of the current study was to develop an approximation for the CIMPLE map solution for short-interval scanning involving the assumption that net intervoxel tumor invasion does not occur within sufficiently short time frames. Proliferation rate maps created using the “no invasion” approximation were found to be increasingly similar to maps created from full solution during increasingly longer follow-up intervals (3D cross correlation, R^2=0.5298, P=0.0001). Results also indicate proliferation rate maps from the “no invasion” approximation had significantly higher sensitivity (82% vs. 64%) and specificity (90% vs. 80%) for predicting six month progression free survival and was a better predictor of time to progression during standard radiochemotherapy compared to the full CIMPLE solution (Log-rank; No Invasion estimation, P=0.0134; Full Solution, P=0.0555). Together, results suggest the “no invasion” approximation allows for quick estimation of proliferation rate using diffusion MRI data obtained from multiple scans obtained daily or biweekly for use in quantifying early treatment response.

Keywords

CIMPLE maps; glioblastoma; GBM; diffusion MRI; ADC; radiochemotherapy; mathematical modeling

Address Correspondence To: Benjamin M. Ellingson, Ph.D. Assistant Professor of Radiology, Biomedical Physics, and Bioengineering UCLA Brain Tumor Imaging Laboratory Department of Radiological Sciences David Geffen School of Medicine University of California – Los Angeles 924 Westwood Blvd, Suite 615 Los Angeles, CA 90024 Phone: (310) 481-7572 Fax: (310) 794-8657 bellingson@mednet.ucla.edu.

Introduction

Diffusion-weighted imaging (DWI) is a useful magnetic resonance imaging technique for assessing early tumor response to treatment [1-3]. The apparent diffusion coefficient (ADC), a measure of free water mobility calculated from DWIs, has been shown to be inversely proportional to tumor cellularity, illustrating a decrease in ADC during growing tumor [4-11] and an increase in ADC during successful chemotherapy [2, 3, 5, 12]. Recently, a new imaging technique was developed termed cell invasion, motility, and proliferation level estimates (CIMPLE maps) [13, 14]. These image maps use a voxel-wise solution to a partial differential equation describing tumor growth dynamics applied to serial ADC maps collected in the same patient over time. By assuming ADC provides a direct measure of tumor cell density, the resultant CIMPLE map solution allows for creation of parametric image maps of "cell diffusion rate" and "cell proliferation rate." Preliminary studies have demonstrated a relationship between proliferation rate estimates and MR spectroscopic estimates of Choline-to-NAA ratio, significant differences in invasion and proliferation rate between high and low grade gliomas [13, 14], and the ability to spatially predict regions of future contrast-enhancement and survival after treatment with bevacizumab [15]. Despite these findings, CIMPLE mapping has practical constraints and limitations that reduce the applicability in certain circumstances.

An inherent limitation to the full CIMPLE map solution is the need for three sequential ADC maps collected in the same patient at follow-up times on the order of months in order to reduce the influence of noise on CIMPLE map parameter estimates. Since cell invasion and proliferation rate estimates are intimately coupled within the CIMPLE map solution, this bias in cell invasion rates also propagates errors in proliferation rate estimates. This temporal constraint further limits the applications of CIMPLE maps to long-term follow-up in brain tumor patients, excluding the possibility of using this technique for characterizing brain tumor growth dynamics within a short interval (days to weeks). Therefore, the objective of the current study was to introduce an approximate solution for estimation of proliferation rates in glioblastoma patients by assuming no detectable tumor cell invasion occurs during short interval follow-ups.

Methods

Derivation of CIMPLE maps

The full derivation of CIMPLE maps is documented elsewhere [13, 14]. Briefly, the net change in tumor cell density in an image voxel can be described by the sum of any net invasion of tumor cells into (or out of) the voxel plus any tumor cells generated (or destroyed) from net proliferation (or degeneration) within the voxel [16, 17]:

$$\overbrace{\frac{dc}{dt}}^{\text{Rate of Change in Cell Density}} = \overbrace{\nabla \cdot (D \nabla c)}^{\text{Invasion}} + \overbrace{\rho \cdot c}^{\text{Proliferation}} \quad \text{[Eq. 2]}$$

where c is cell density, D is the diffusion coefficient of migrating cells, is the cell proliferation rate, and t is time. Based on evidence of a strong negative correlation between tumor cell density and ADC of water measured using DWI [4-7, 9-11], ADC can be substituted into Eq. 1 to yield a mathematical relationship describing microscopic glioma growth and invasion in terms of water mobility:

$$\frac{d}{dt} ADC = D\tilde{\nabla}^2 ADC + \tilde{\nabla} D \times \tilde{\nabla} ADC + \rho \times ADC \quad \text{[Eq. 3]}$$

where *ADC* is the apparent diffusion coefficient of water as a three-dimensional scalar field (i.e. ADC image volume acquired using DWI), *D* is the diffusion coefficient of migrating cells as a three-dimensional scalar field, and is the cell proliferation rate as a three-dimensional scalar field.

An analytical expression for cell diffusion rate, *D*, and proliferation rate, , can be described by using the Methods of Characteristics [18] to achieve one possible solution:

$$D=\frac{\frac{d}{dt}ADC^{n}-\lambda\frac{d}{dt}ADC^{n-1}}{\tilde{\nabla}^{2}ADC^{n}-\lambda\tilde{\nabla}^{2}ADC^{n-1}} \quad \text{[Eq. 4]}$$

and

$$\rho=\rho^{n-1}=-\frac{1}{ADC^{n-1}}\left(\frac{d}{dt}ADC^{n-1}-D\nabla^{2}ADC^{n-1}-\nabla D\cdot\nabla ADC^{n-1}\right) \quad \text{[Eq. 5]}$$

where

$$\frac{d}{dt}ADC^{n-1}=\frac{ADC^{n-1}-ADC^{n-2}}{t^{n-1}-t^{n-2}} \quad \text{[Eq. 6]}$$

describes the time-rate of change in ADC and

$$\lambda=\frac{ADC^{n}}{ADC^{n-1}} \quad \text{[Eq. 7]}$$

describes the ratio of ADC on the current day *n* with respect to the previous scan day *n-1*. Thus, using three ADC maps collected on days t^{n}, t^{n-1}, and t^{n-2}, the proliferation rate, , and cell motility (diffusion), *D*, can be directly estimated for the time interval spanned from t^{n-2} to t^{n} using Eqs. 4-7. Analytical solutions to the glioma growth model were verified in Mathematica v7.01 (Wolfram Mathematica 7.01, Wolfram Research, Inc, Champaign, IL) and are further defined in a previous publication [14].

Proliferation Rate Estimates During Short-Interval Follow-up

The net velocity (*v*, in *mm/yr*) of an invading tumor cell wavefront can be estimated by knowing the migration rate, *D*, and proliferation rate, :

$$\nu=\sqrt{D\cdot\rho} \quad \text{[Eq. 8]}$$

Based on our experience, we can assume a cell invasion rate of 100 mm^{2}/yr and a proliferation rate of nearly 10 yr^{-1} occurs in a cluster of a moderately aggressive glioblastoma. A simple estimate of the invasion velocity results in approximately 31.6 *mm/yr*. Using the previous limitations and suggestions for follow-times, an interval of 30 days between scans (or 60 days total observation time for three scans) results in a bulk invasion distance of 5.2 *mm*, or more than 5 voxels after interpolation and registration to 1mm isotropic resolution. Alternatively, if ADC maps are collected with follow-up times of two days (total of four days for all three scans), the bulk invasion distance is only approximately 0.3 *mm*, or less than a single voxel. Ergo, a solution that excludes the contributions of intervoxel tumor invasion may be appropriate for exploring tumor dynamics for very short interval follow-up.

Exclusion of the invasion term, *D*, from the full microscopic glioma growth model shown in Eq. 3 results in a simple first-order, linear differential equation,

$$\frac{d}{dt}ADC = \rho \cdot ADC \quad \text{[Eq. 9]}$$

with the monoexponential solution

$$ADC(t) = ADC(0) \cdot e^{-\rho \cdot t} \quad \text{[Eq. 10]}$$

Note that in Eq. 10 the sign on the proliferation rate estimate, , is positive for decreasing ADC (i.e. increasing cell density). Physically, voxels containing a high positive proliferation rate represent voxels having a very rapid decrease in ADC over the time interval of observation, whereas voxels containing a high *negative* proliferation rate (or "degeneration rate") represents voxels having a very rapid *increase* in ADC over the time interval of observation.

Patient Population

All patients in this study signed institutional review board-approved informed consent to have their data collected and stored in our institution's neurooncology database. Data acquisition and storage were performed in compliance with all applicable Health Insurance Portability and Accountability Act (HIPAA) regulations. A total of $n = 22$ patients were selected from our database having the following criteria: 1) a primary histological diagnosis of de novo glioblastoma from 1/1/2007 through 1/1/2011, 2) receiving radiation therapy and concurrent temozolomide after resection at initial diagnosis, 3) having a minimum of three follow-up scans including: a) post-surgical, pre-radiochemotherapy, b) mid-radiochemotherapy, and c) post-radiochemotherapy not spanning more than a total of eight months (note that all post-radiochemotherapy scans were obtained *prior* to radiographic progression), and 4) sufficient quality diffusion MRI data (e.g. lack of severe geometric distortions, adequate signal-to-noise ratio in raw diffusion MR images, and ADC values in cerebrospinal fluid ranging from 2-3 um^2/ms). Fig. 1 illustrates the experimental timeline for the three scans used to calculate CIMPLE maps.

Magnetic Resonance Imaging

Data was collected on a 1.5T MR system (General Electric Medical Systems, Waukesha, WI; or Siemens Medical; Erlangen, Germany) using pulse sequences supplied by the scanner manufacturer. Standard anatomical MRI sequences included axial T1 weighted, T2 weighted, and fluid attenuated inversion recovery (FLAIR) images. DWIs were collected with TE/TR = 102.2 ms/8000 ms, NEX = 1, slice thickness = 5 mm with 1 mm interslice distance, matrix size = 128 × 128 and a FOV = 24 cm using a twice-refocused SE-EPI preparation [19]. ADC images were calculated from acquired DWIs with b = 1,000 s/mm^2 and b = 0 s/mm^2 images. Additionally, gadopentetate dimeglumine enhanced (Magnevist; Berlex, Wayne, NJ; 0.1 mmol/kg) axial and coronal T1 weighted images were acquired after contrast injection.

Definition of Disease Progression

Progression was defined prospectively by the treating neuro-oncologists. In an effort to decrease the likelihood of declaring progression in the setting of pseudoprogression, the post-radiation scan was considered the baseline scan for evaluating progression. If subsequent scans showed definite increase in imaging evaluable tumor (≥25% increase in the sum of enhancing lesions, new enhancing lesions greater than $1cm^2$, or an unequivocal qualitative increase in non-enhancing tumor, or unequivocal new area of non-contrast enhancing tumor), progression was declared at that time. Progression was determined using the first post-radiation therapy scan only if a new lesion, greater than $1cm^2$, was identified

outside the radiation field. Change in steroid dosage was taken into consideration before defining progression. Patients who did not meet these imaging criteria for progression, but had significant neurologic decline, were declared progressed at the time of irreversible decline. Patients who died before evidence of imaging progression were defined progressed on the date of death.

Image Registration

All images for each patient were independently registered to a high-resolution (1.0 mm isotropic), T1-weighted brain atlas (MNI152; Montreal Neurological Institute) using a mutual information algorithm and a 12-degree of freedom transformation using FSL (FMRIB, Oxford, UK; http://www.fmrib.ox.ac.uk/fsl/). Fine registration (1–2 degrees and 1–2 voxels) was then performed using a Fourier transform-based, 6-degree of freedom, rigid body registration algorithm [20] followed by visual inspection to ensure adequate alignment.

Regions of Interest (ROIs)

Regions of interest (ROIs) containing T2 weighted signal abnormality on pre-treatment FLAIR images were used in subsequent analyses. These ROIs were defined by a technologist (T.M.Z.) using a semi-automated ROI technique consisting of (1) manually defining the relative region of tumor occurrence, (2) thresholding FLAIR images within these regions using an empirical threshold combined with a region-growing algorithm, and then (3) manually editing the resulting masks to exclude any obvious radiation-induced changes, necrosis, gliosis or leukoaraiosis. by a board-certified neuroradiologist (W.B.P.) and/or imaging scientist (B.M.E.).

Implementation and analysis of CIMPLE maps

The creation of CIMPLE maps was incorporated into an AFNI pipeline (AFNI, Analysis of Functional Neuroimages; http://afni.nimh.nih.gov/afni) using a combination of bash and AFNI calculation commands. Nearest neighbor interpolation was implemented in AFNI and used to estimate the spatial gradients of ADC. Resulting cell diffusion coefficient maps, D, and proliferation rate maps, ρ, were smoothed using a 3×3 median filter to eliminate erroneous spikes in the image maps. Proliferation maps generated without invasion were obtained by nonlinear least-squares regression, fitting Eq. 10 on a voxel-wise basis to the experimental data. Nonlinear least-squares regression was implemented using the *3dNLfim* routine in AFNI.

The final quantitative maps of proliferation rate, ρ, were generated using a minimum contiguous cluster size of 0.2 ml, thresholded above an absolute proliferation rate value of 2 $year^{-1}$, in order to eliminate erroneous voxels and better isolate the region(s) of proliferative tumor. For proliferation rate estimates assuming “no invasion”, voxels containing a p-value of less than 0.05 from nonlinear regression were retained. The average proliferation rate within these ROIs were recorded and compared as potential predictors of progression-free survival (PFS).

Hypothesis Testing

In order to assess the spatial similarities between proliferation rate estimates using the full CIMPLE map solution and proliferation rate estimates obtained using the simplified “no invasion” approximation, the three-dimensional cross-correlation was calculated for each patient. To test whether the degree of overlap between the two techniques differed as a function of the shortest follow-up interval between sequential scans (e.g. either between pre- and mid-radiochemotherapy or between mid- and post-radiochemotherapy), linear

regression was performed between follow-up times and the three-dimensional cross-correlation.

The sensitivity and specificity for mean proliferation rate to predict six month progression-free survival (PFS6) was compared between the two techniques using receiver-operator characteristics (ROC) and the area under the curve (AUC). Given the optimal threshold for maximizing sensitivity and specificity for PFS6, log-rank analysis was performed on Kaplan-Meier data to determine if either technique was a significant predictor of time to progression (TTP).

Results

In general, proliferation rate images were similar when comparing the full CIMPLE mapping solution with the "no invasion" approximation (Fig. 2). Specifically, regions of positive and negative proliferation rate were spatially localized to similar regions using each technique, including similar regions of positive proliferative tissue on the edge of contrast enhancement and within T2 signal abnormality. In support of the qualitative similarity between the two solutions, three-dimensional cross correlation increased significantly with increasing minimum follow-up interval (Fig. 3; *Pearson's Correlation Coefficient,* $R^2=0.5298$, *P=0.0001*). In other words, as the minimum time interval between ADC maps increased, the contributions to noise on estimates of cell motility rate were likely lower, and the full solution for proliferation rate tended to converge with the "no invasion" approximation. According to the best-fit regression line, convergence of proliferation rate estimates from the full solution and "no invasion" approximation should occur around minimum follow-up time of 66 days or more.

Mean proliferation rate estimates from the full CIMPLE solution did not have significant sensitivity and specificity for predicting PFS6 beyond that of chance according to ROC analysis (Fig. 4A; *AUC vs. Chance, t-test, P=0.3981*). However, the mean proliferation rates estimated from the "no invasion" approximation demonstrated significantly higher sensitivity and specificity for predicting PFS6 beyond that of chance (*AUC vs. Chance, t-test, P=0.0113*). The AUC was significantly different between the two techniques (Fig. 4B; $AUC_{Full\ Solution}$ *vs.* $AUC_{"No\ Invasion"}$, *t-test, P=0.0412*), supporting the hypothesis that a "no invasion" approximation may perform better as a predictive tool compared with the full CIMPLE solution under this particular experimental setup and treatment paradigm.

Although not a significant predictor of PFS6 using ROC analysis, the optimal threshold for the proliferation rate using the full solution was 4.2 yr^{-1}, resulting in a 64% sensitivity and 80% specificity for PFS6. The optimal threshold for proliferation rate using the "no invasion" approximation was 2.25 yr^{-1}, resulting in a 82% sensitivity and 90% specificity for PFS6. Using these thresholds to stratify patients into two groups, log-rank analysis suggested a trend for significant differences between high and low proliferation rate groups when implementing the full solution (Fig. 5; *Log-rank, P=0.0555; High, Median PFS=117 days; Low, Median PFS=278 days*); however, log-rank analysis clearly demonstrated a statistically significant PFS advantage for patients with low proliferation rate when using the "no invasion" approximation (*Log-rank, P=0.0134; High, Median PFS=127 days; Low, Median PFS=282 days*). Despite a slightly better performance by the proliferation rate estimate obtained using the "no invasion" approximation, hazard ratios were not significantly different between the two solutions.

Discussion

CIMPLE mapping is a unique imaging technique that provides a comprehensive framework for creating parametric maps of microscopic invasion and proliferation rate estimates using serial diffusion MRI. However, a few practical constraints have limited the use of CIMPLE maps as a tool for estimating these dynamic parameters, particularly during short-interval follow-up times. Previous investigations examining the contributions of noise and follow-up interval on these parameters have firmly demonstrated an increase in error for increasing noise levels and decreasing interval follow-up times [15]. As the time interval between follow-up ADC maps is shortened, noise in the ADC map may be interpreted as very fast movement of tumor cells. Conversely, if the time interval between follow-up ADC maps is lengthened, the resulting error in parameter estimates from noise present in the ADC map are low enough to be excluded by filtering or thresholding the resulting maps. By arguing the point that cell invasion velocities may not be high enough to migrate a substantial distance during short intervals, we present a practical solution for estimating proliferation rate on a voxel-wise basis by excluding the contribution of cell migration and invasion from the CIMPLE mapping equation.

Results from the current study demonstrate that proliferation rate maps generated using the full CIMPLE mapping solution appear similar to proliferation rate maps generated using the “no invasion” approximation as illustrate by increasing three-dimensional spatial agreement with an increasing time interval between follow-up scans. Additionally, results indicate the “no invasion” approximation may also be a better predictor of PFS and TTP when using preradiochemotherapy, mid-radiochemotherapy, and post-radiochemotherapy scans as to predict standard treatment response.

Interestingly, if the contributions to tumor cell motility and invasion are excluded from the model, an estimate of proliferation rate can be obtained using a *minimum of two* time points using the following equation:

$$\rho = -\frac{1}{t}\ln\left(\frac{ADC(t)}{ADC(0)}\right) \quad \text{[Eq. 11]}$$

Further, the “no invasion” approximation of proliferation rate is not necessarily limited by the time interval between scans, since accuracy can be increased directly by increasing the number of follow-up time points even in short intervals (e.g. days). It is conceivable that an imaging paradigm consisting of daily or biweekly scanning for the first few weeks of therapy may be advantageous to obtain the best estimates of proliferation rate for use in quantifying treatment response.

Methodological and Study Limitations

The major limitations to estimating proliferation rates using the full CIMPLE map solution include the assumption that DWI measurement of ADC is inversely proportional with tumor cellularity along with the reliance of precise image registration of serial images from different scan days. Although numerous studies have demonstrated a significant association between tumor cellularity and ADC, many pathologies and clinical scenarios can also alter ADC measurements, including subacute stroke, gliosis, and changes in corticosteroid dose. Therefore, interpretation of changes in ADC as true changes in cellularity should be made with caution. Experience at our institution suggests significant changes in edema (increasing or decreasing) can significantly alter proliferation rate estimates obtained using CIMPLE mapping. In addition to altered estimates of ADC, brain deformation resulting from significant mass effect from growing tumor or edema can cause misregistration between serial ADC maps and anatomical images. Practically, this implies ADC maps should be

obtained in a short enough time interval such that no significant mass effect has occurred. In addition, significant mass effect (>5mm shift in the midline) was not directly observed in any of the patients and was thought to be of minimal contribution to errors in parameter estimates.

Another potential limitation to the current study was the lack of adjustment of survival analyses for known prognostic factors including patient age, extent of resection, and neurological status. We did not currently test whether CIMPLE map parameters added value beyond these known prognostic factors due to the relatively small sample size. Future prospective studies examining larger patient populations under controlled image acquisition and follow-up time intervals are necessary to determine whether CIMPLE maps provide a true prognostic benefit.

Conclusion

The current study demonstrates a new method for estimating proliferation rate for short-interval follow-up scans by excluding the contributions intervoxel tumor cell invasion. The “no invasion” approximation was similar to the full solution for increasing follow-up interval times, and may be a better predictor of response to radiochemotherapy than the full solution, particularly when short-interval follow-up scanning is used.

Acknowledgments

Grant Support: NIH/NCI R21CA167354 (BME); UCLA Institute for Molecular Medicine Seed Grant (BME); UCLA Radiology Exploratory Research Grant (BME); University of California Cancer Research Coordinating Committee Grant (BME); ACRIN Young Investigator Initiative Grant (BME); Art of the Brain (TFC); Ziering Family Foundation in memory of Sigi Ziering (TFC); Singleton Family Foundation (TFC); Clarence Klein Fund for Neuro-Oncology (TFC)

References

1. Padhani AR, Liu G, Mu-Koh D, Chenevert TL, Thoeny HC, Takahara T, DzikJurasz A, Ross BD, Van Cauteren M, Collins D, Hammoud DA, Rustin GJS, Taouli B, Choyke PL. Diffusion-weighted magnetic resonance imaging as a cancer biomarker: consensus and recommendations. Neoplasia. 2009; 11:102–125. [PubMed: 19186405]
2. Chenevert TL, McKeever PE, Ross BD. Monitoring early response of experimental brain tumors to therapy using diffusion magnetic resonance imaging. Clinical Cancer Research. 1997; 3:1457–1466. [PubMed: 9815831]
3. Provenzale JM, Mukundan S, Barboriak DP. Diffusion-weighted and perfusion MR imaging for brain tumor characterization and assessment of treatment response. Radiology. 2006; 239:632–649. [PubMed: 16714455]
4. Sugahara T, Korogi Y, Kochi M, Ikushima I, Shigematu Y, Hirai T, Okuda T, Liang L, Ge Y, Komohara Y, Ushio Y, Takahashi M. Usefulness of diffusion-weighted MRI with echo-planar technique in the evaluation of cellularity in gliomas. J Magn Reson Imaging. 1999; 9:53–60. [PubMed: 10030650]
5. Chenevert TL, Stegman LD, Taylor JM, Robertson PL, Greenberg HS, Rehemtulla A, Ross BD. Diffusion magnetic resonance imaging: an early surrogate marker of therapeutic efficacy in brain tumors. J Natl Cancer Inst. 2000; 92:2029–2036. [PubMed: 11121466]
6. Lyng H, Haraldseth O, Rofstad EK. Measurements of cell density and necrotic fraction in human melanoma xenografts by diffusion weighted magnetic resonance imaging. Magn Reson Med. 2000; 43:828–836. [PubMed: 10861877]
7. Hayashida Y, Hirai T, Morishita S, Kitajima M, Murakami R, Korogi Y, Makino K, Nakamura H, Ikushima I, Yamura M, Kochi M, Kuratsu JI, Yamashita Y. Diffusion-weighted imaging of metastatic brain tumors: comparison with histologic type and tumor cellularity. AJNR Am J Neuroradiol. 2006; 27:1419–1425. [PubMed: 16908550]

8. Manenti G, Di Roma M, Mancino S, Bartolucci DA, Palmieri G, Mastrangeli R, Miano R, Squillaci E, Simonetti G. Malignant renal neoplasms: correlation between ADC values and cellularity in diffusion weighted magnetic resonance imaging at 3 T. Radiologia Medica. 2008; 113:199–213. [PubMed: 18386122]
9. Gauvain KM, McKinstry RC, Mukherjee P, Perry A, Neil JJ, Kaufman BA, Hayashi RJ. Evaluating pediatric brain tumor cellularity with diffusion-tensor imaging. AJR Am J Roentgenol. 2001; 177:449–454. [PubMed: 11461881]
10. Kinoshita M, Hashimoto N, Goto T, Kagawa N, Kishima H, Izumoto S, Tanaka H, Fujita N, Yoshimine T. Fractional anisotropy and tumor cell density of the tumor core show positive correlation in diffusion tensor magnetic resonance imaging of malignant brain tumors. Neuroimage. 2008; 43:29–35. [PubMed: 18672074]
11. Kono K, Inoue Y, Nakayama K, Shakudo M, Morino M, Ohata K, Wakasa K, Yamada R. The role of diffusion-weighted imaging in patients with brain tumors. AJNR Am J Neuroradiol. 2001; 22:1081–1088. [PubMed: 11415902]
12. Stegman LD, Rehemtulla A, Hamstra DA, Rice DJ, Jonas SJ, Stout KL, Chenevert TL, Ross BD. Diffusion MRI detects early events in the response of a glioma model to the yeast cytosine deaminase gene therapy strategy. Gene Ther. 2000; 7:1005–1010. [PubMed: 10871748]
13. Ellingson BM, Rand SD, Malkin MG, Prost R, Connelly JM, LaViolette PS, Bedekar DP, Schmainda KM. Spatially quantifying microscopic tumor invasion and proliferation using a voxel-wise analytical solution to a glioma growth model and serial diffusion MRI. Proc Intl Soc Mag Reson Med. 2010; 18:612.
14. Ellingson BM, LaViolette PS, Rand SD, Malkin MG, Connelly JM, Mueller WM, Prost RW, Schmainda KM. Spatially Quantifying Microscopic Tumor Invasion and Proliferation Using a Voxel-Wise Solution to a Glioma Growth Model and Serial Diffusion MRI. Magn Reson Med. 2011; 65:1132–1144.
15. Ellingson BM, Cloughesy TF, Lai A, Nghiemphu PL, Pope WB. Cell invasion, motility, and proliferation level estimate (CIMPLE) maps derived from serial diffusion MR images in recurrent glioblastoma treated with bevacizumab. J Neurooncol. 2011; 105:91–101. [PubMed: 21442275]
16. Swanson KR, Alvord EC Jr. Murray JD. A quantitative model for differential motility of gliomas in grey and white matter. Cell Prolif. 2000; 33:317–329. [PubMed: 11063134]
17. Harpold HL, Alvord EC Jr. Swanson KR. The evolution of mathematical modeling of glioma proliferation and invasion. J Neuropathol Exp Neurol. 2007; 66:1–9. [PubMed: 17204931]
18. Farlow, SJ. Partial differential equations for scientists and engineers. Wiley; New York: 1993.
19. Reese TG, Heid O, Weisskoff RM, Wedeen VJ. Reduction of eddy-current-induced distortion in diffusion MRI using a twice-refocused spin echo. Magnetic Resonance in Medicine. 2003; 49:177–182. [PubMed: 12509835]
20. Cox RW, Jesmanowicz A. Real-time 3D image registration for functional MRI. Magn Reson Med. 1999; 42:1014–1018. [PubMed: 10571921]

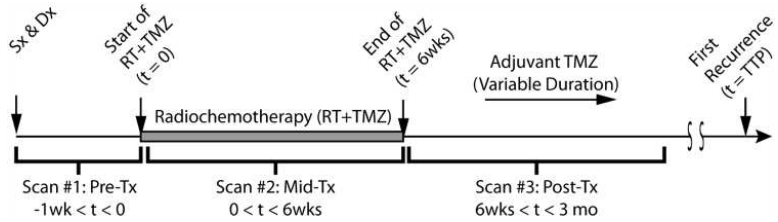

Figure 1. Experimental design for predicting response to radiochemotherapy using CIMPLE maps.

Scans were obtained 1) post-surgical (Sx), pre-treatment (Pre-Tx; within 1 week of starting radiochemotherapy); 2) mid-treatment (Mid-Tx, 0 – 6 wks from start of radiochemotherapy); and post-treatment (Post-Tx; 6 wks to 3 months from the start of radiochemotherapy). Sx = Surgery. Dx = Diagnosis. Tx = Treatment. RT = Radiotherapy. TMZ = Temozolomide. TTP = Time to Progression.

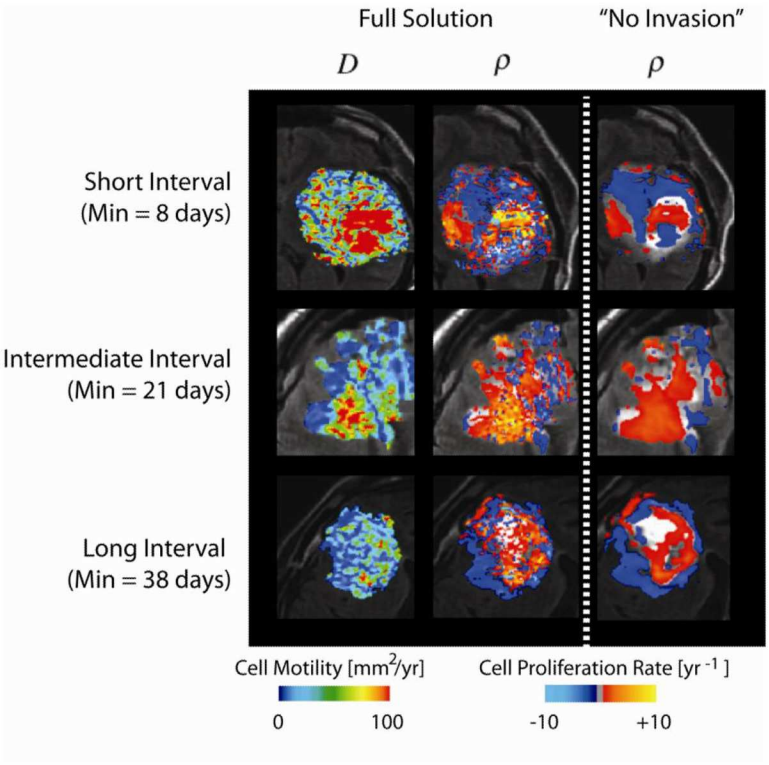

Figure 2. Comparison between full CIMPLE map solution and "no invasion" approximation.
Top row: Glioblastoma patient with an 8 day follow-up interval (between pre-treatment and mid-treatment), demonstrating high cell motility (diffusion) rates and spatial uncoupling between the two solutions in terms of proliferation rate estimates. Middle row: Glioblastoma patient with a 21 day follow-up interval demonstrating lower average cell motility rate and proliferation rate estimates with higher spatial agreement between the two solutions. Bottom row: Glioblastoma patient with a 38 day interval, representing one of the longest obtainable follow-up times given the experimental design in Fig. 1. This patient demonstrated high spatial agreement in proliferation rate maps when comparing between the two techniques (full solution vs. "no invasion").

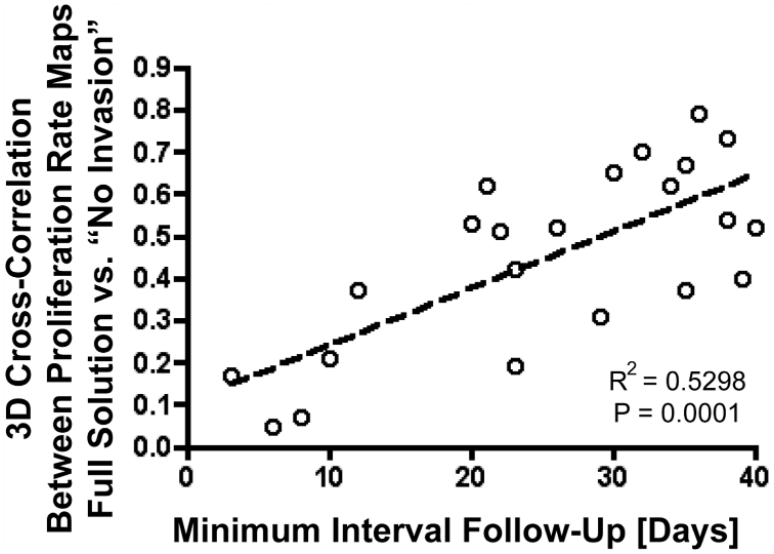

Figure 3. Three-dimensional cross-correlation between proliferation rate maps obtained with the full solution and those obtained with the "no invasion" approximation.

Results demonstrate a significant linear correlation between the three-dimensional cross-correlation coefficient and the shortest time interval between sequential ADC maps (*Pearson's correlation coefficient,* $R^2 = 0.5298$, $P = 0.0001$).

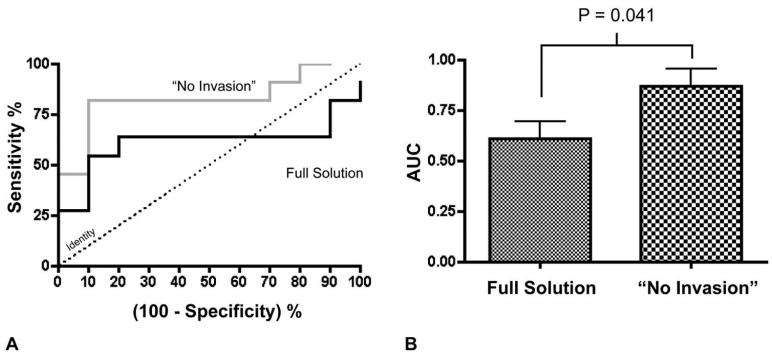

Figure 4. Receiver-operator characteristic (ROC) analysis of the ability for mean proliferation rate to predict six-month progression free survival (PFS6).

A) ROC curves showing the sensitivity and specificity for predicting PFS6 for both the full CIMPLE map solution and the "no invasion" approximation. B) Area under the curve (AUC) showing statistically significant differences between the two techniques (*t*-test, $P = 0.041$).

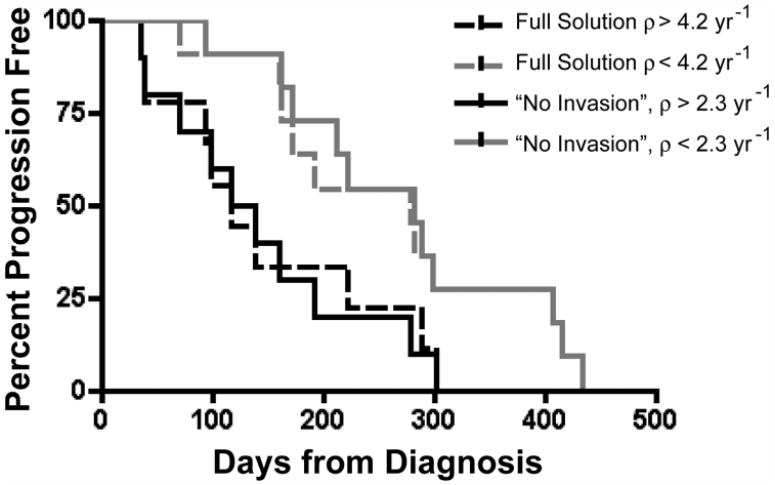

Figure 5. Kaplan-Meier progression free survival (PFS) curves for high and low mean proliferation subgroups from both the full CIMPLE map solution and the "no invasion" approximation.

Patients were stratified into two groups based on whether the mean proliferation rate within T2 hyperintense regions was higher or lower than the optimal threshold determined by ROC analysis for both techniques (full solution vs. "no invasion"). Patients with high mean proliferation rate were more likely to progress sooner than patients with low proliferation rate when using the "no invasion" approximation (*Log-rank, P =0.0134*). This was also a trend when using the full solution (*Log-rank, P = 0.0555*).